Solid-State Electronics 83 (2013) 113–117

Contents lists available at SciVerse ScienceDirect

Solid-State Electronics

journal homepage: www.elsevier.com/locate/sse

Terahertz imaging using strained-Si MODFETs as sensors

Y.M. Meziani [a], E. Garcìa-Garcìa [a,1], J.E. Velázquez-Pérez [a,*], D. Coquillat [b], N. Dyakonova [b], W. Knap [b], I. Grigelionis [c], K. Fobelets [d]

[a] Dpto. de Fĺsica Aplicada, Universidad de Salamanca, E-37008 Salamanca, Spain
[b] Laboratoire Charles Coulomb, UMR 5221 CNRS-Université Montpellier 2, Montpellier 34095, France
[c] Institute of Experimental Physics, University of Warsaw, 00-681 Warsaw, Poland
[d] Department of Electrical and Electronic Engineering, Imperial College, London SW7 2AZ, UK

ARTICLE INFO

Article history:
Available online 26 February 2013

Keywords:
Terahertz
SiGe
MODFET
Imaging
Sensors

ABSTRACT

We report on non-resonant (broadband) and resonant detection of terahertz radiation using strained-Si modulation doped field effect transistors. The devices were excited at room temperature by two types of terahertz sources (an electronic source based on frequency multipliers at 0.292 THz and a pulsed parametric laser at 1.5 THz). In both cases, a non-resonant response with maxima around the threshold voltage was observed. Shubnikov-de Haas and photoresponse measurements were performed simultaneously and showed a phase-shift of $\pi/2$ in good agreement with the theory, which demonstrates that the observed response is related to the plasma waves oscillation in the channel. The non-resonant features were used to demonstrate the capabilities of such devices in terahertz imaging. We also cooled our device down to 4.2 K to increase the quality factor and resonant detection was observed by using a tunable source of terahertz radiation.

1. Introduction

Nowadays, terahertz (THz) technology is increasingly attracting interest due to its potential in many different applications like medical diagnostics, product quality control, and security screening. Terahertz rays are located in the spectral region 0.1–10 THz (~3 mm–30 μm, 3–300 cm^{-1}) between the microwave and the infrared portion of the electromagnetic spectrum [1]. An excellent review, highlighting the importance of terahertz radiation in different types of applications from astronomy to spectroscopy, can be found in [2] and references therein. The attractive features of THz radiation for applications are the following: (i) they can penetrate cloths and most packaging materials such as paper or plastics, (ii) many substances have "fingerprint" spectra in the THz range, and (iii) due to its low photon energy (about one million times less than X-rays), THz radiation is non-ionizing and therefore not dangerous for human beings. These properties make THz systems a promising tool for different types of applications wherever detection and identification of hidden threats is the task and when human beings are to be scanned.

In early 1990s, Dyakonov and Shur [3] theoretically demonstrated the possibility of using sub-micron field effect transistors as detectors of terahertz radiation by means of the oscillations of plasma waves in their channel. Those devices present many advantages: low cost, small size, room temperature operation, and tuning of the resonant frequency by the electron density (i.e., the gate voltage). Experimental investigations have been conducted on different types of transistors, demonstrating their capabilities for detection of terahertz radiation. Resonant detection using GaAs/AlGaAs FETs[2] was reported by Knap et al. [4] at 8 K. Later, they reported non-resonant detection [5] at room temperature. Knap et al. [6] demonstrated, in 2004, room temperature non-resonant detection by using silicon FETs where responsivity lower than 200 V/W and a Noise Equivalent Power (NEP) of around 1 $pW/Hz^{1/2}$ [7,8] were estimated. Terahertz imaging based on CMOS technology has been reported by different groups [9,10]. Recently, a responsitivity of 80 kV/W and a NEP of 300 $pW/Hz^{1/2}$ as well as imaging at 0.65 THz were reported using an array of Si-MOSFET processed by 0.25 μm CMOS technology [11].

The paper is organized as follows: In Section 2, the strained-silicon modulation doped field effect transistors (MODFET), used in the experiments, are described. In Section 3, non-resonant detection is reported for different gate length devices and using different sources of terahertz radiation. Simultaneously performed Shubnikov-de-Haas and response measurements under magnetic field show that the observed response is explained as due to the oscillations of the plasma waves in the channel. Section 4 is dedicated to the performance of these devices when used as sensors in a

* Corresponding author.
E-mail address: js@usal.es (J.E. Velázquez-Pérez).
[1] Also at: Centro de Láseres Pulsados (CLPU), Salamanca, Spain.

[2] FET: Field Effect Transistor.

0038-1101/$ - see front matter © 2013 Elsevier Ltd. All rights reserved.
http://dx.doi.org/10.1016/j.sse.2013.01.030

terahertz imaging system. In the last section (Section 5), we show some signature of a resonant detection from our device where the resonant frequency shifts accordingly to the Dyakonov–Shur theory.

2. Strained-silicon MODFET

The epistructure of the MODFETs used in this work was grown by molecular beam epitaxy (MBE) on a thick relaxed SiGe virtual substrate grown by low-energy plasma-enhanced chemical vapor deposition (LEPECVD) over a p-doped conventional Si wafer. The final Ge molar concentration in the virtual substrate was $x_{Ge} = 0.45$. The device had a 8 nm tensile strained (in terms of biaxial deformation) Si channel, sandwiched between two heavily doped SiGe electron supply layers to generate a high carrier density in the strained-Si quantum well [12]. The ohmic contacts were not self-aligned. Two transistors with different gate lengths (50 nm and 250 nm) were used in measurements. The gate width and the source-to-drain length were 30 μm and 1 μm, respectively. The left part of Fig. 1a shows the epistructure as well as the energy band diagram of the MODFET calculated using MEDICI™ [12]. The right part shows a SEM image of a transistor where drain, gate, and source pads are highlighted. This double-doped MODFET exhibits a large off-current and cannot be switched off within a practical gate voltage range.

3. Non-resonant response

Fig. 2 shows the photoresponse signal for a device with $L_g = 250$ nm and for two different fixed drain-to-source voltages ($V_{ds} = 0.5$, 1.5 V). The device was excited at room temperature by a terahertz wave parametric oscillator (TPO) pulsed laser at 1.5 THz [13]. The TPO can emit quasi-monochromatic Terahertz-waves over a wide tunable frequency range from 0.4 THz to 2.8 THz with a narrow line-width lower than 100 MHz, via optical rectification. The output power of the laser was 6 nJ/pulse for the range 1.3–1.6 THz and a repetition rate of 500 Hz. The incoming radiation intensity was modulated by a mechanical chopper at 1.29 kHz and coupled to the device via the metallization pads. The induced photoresponse signal was measured by using a lock-in amplifier technique. More description of the experimental setup can be found in [7]. The signal intensity increases with the drain current as predicted by the theory [14,15], showing a maximum around the threshold voltage. The responsivity was estimated to be 25 V/J/Pulse at $V_{ds} = 1.5$ V.

Fig. 3 shows the photoresponse signal obtained for a small device with $L_g = 50$ nm when excited by an electronic source based on frequency multipliers at 0.292 THz with power around 5 mW.

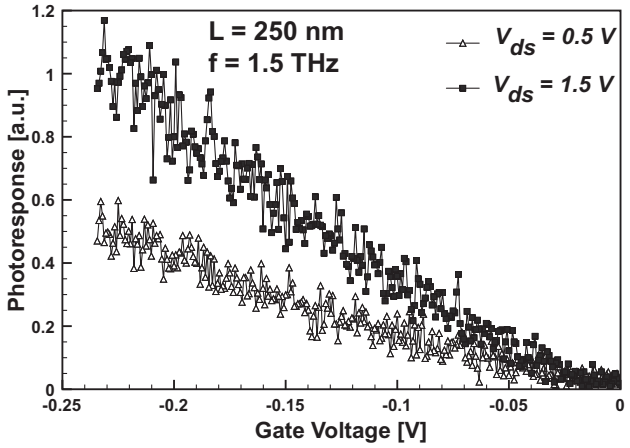

Fig. 2. Photoresponse vs gate bias for a device with $L_g = 250$ nm excited at 1.5 THz and under source-to-drain bias of 0.5 V and 1.5 V.

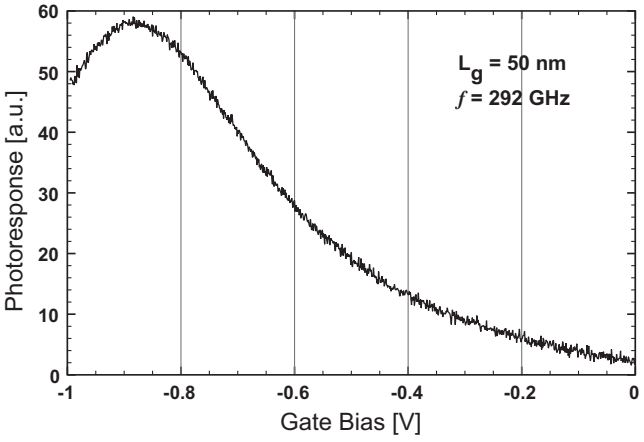

Fig. 3. Measured photoresponse signal of the device as function of the gate voltage at room temperature. The curve shows a maximum near to the threshold voltage of the MODFET.

Since the power is higher and the device is smaller than in the previous experiment, the photoresponse is more pronounced and a clear maximum is observed around $V_{th} = -0.84$ V. A maximum of the signal is clearly observed around the threshold voltage for both cases (Figs. 2 and 3), even if the excitation frequency was different. This behavior has been reported earlier and explained as non-resonant detection due to a low value of the quality factor ($Q = \omega\tau < 1$) [6,12], that is, a low mobility in the device's channel. In the present

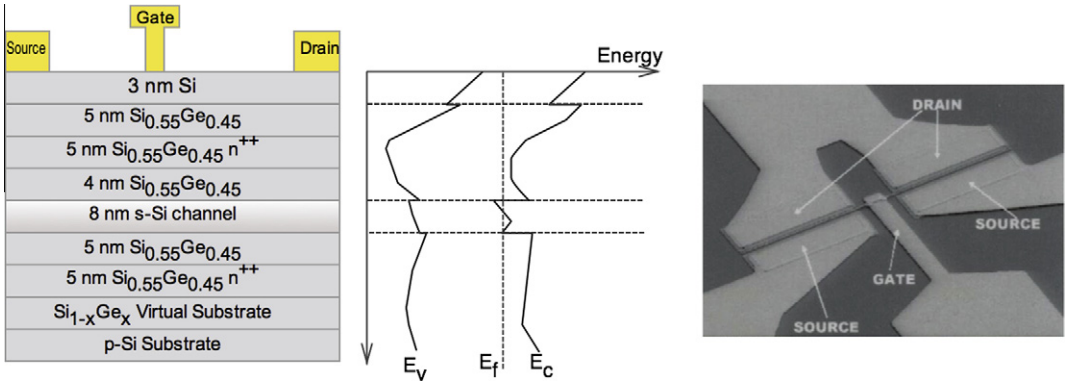

Fig. 1. Left: Epistructure of the MODFET as well as the energy band diagram [12]. Right: SEM image of a transistor where drain, gate, and source pads are highlighted.

case, the device shows higher channel mobility (~1355 $cm^2/V\,s$) as compared to the conventional Si-MOSFET (~200 $cm^2/V\,s$) and the quality factor was estimated around 1.2 at $f = 1.5$ THz and around 0.27 at $f = 0.292$ THz. Those values are higher than in pure silicon FETs; however, no resonance is observed probably due to the low-efficiency coupling of the incoming radiation. Rumyantsev et al. [12] obtained a maximum value of the photoresponse signal when the beam was focused away from the transistor on similar devices. This has been presented as a proof of the low coupling of the incident terahertz radiation to the device's channel. Dependence of the photoresponse on the polarization of the incoming radiation was reported recently by Meziani et al. [16] where a maximum response was observed when the light was polarized along the channel. Terahertz photon helicity sensitive photoresponse has been reported recently in similar devices [17] and was explained as due to the interferences of the plasma oscillations in the channel.

Dyakonov et al. [18] demonstrated theoretically a phase-shift of $\pi/2$ between Shubnikov-de-Haas oscillations and photoresponse oscillations under high magnetic field intensity. The photoresponse (ΔU) is given by:

$$\Delta U = \frac{1}{4}\frac{U_a^2}{U_0}\left[f(\beta) - \frac{\partial\gamma}{\partial n}\frac{n}{\gamma}g(\beta)\right] \tag{1}$$

where U_a is the amplitude of the modulation of the gate-to-source voltage due to the external radiation, U_0 is the dc value of the gate–source voltage, n the electron concentration in the channel and $\beta = \omega_c/\omega$ (ω_c and ω are the cyclotron resonance and the incoming radiation frequency respectively). The dependence of the photoresponse on the magnetic field and the radiation frequency is described by the functions $f(\beta)$ and $g(\beta)$:

$$f(\beta) = 1 + \frac{1+F^2}{\sqrt{\alpha^2+F^2}} \tag{2}$$

$$g(\beta) = \frac{1+F}{2}\left(1 + \frac{1+F^2}{\sqrt{\alpha^2+F^2}}\right) \tag{3}$$

$$F = \frac{1+\alpha^2-\beta^2}{1+\alpha^2+\beta^2} \quad \text{and} \quad \alpha = (\omega\tau)^{-1} \tag{4}$$

The γ factor is an oscillating function of the magnetic field and the electron concentration that can be correlated with the Shubnikov-de-Haas oscillations. The first term in Eq. (1) is related to the contribution of the cyclotron resonance. The second term is responsible for the oscillations and is proportional to $\partial\gamma/\partial n$, or, to $\partial\gamma/\partial B$, thus resulting in a $\pi/2$ phase-shift, which we observe experimentally. Fig. 4 shows the Shubnikov-de-Haas oscillations (right axis) and the photoresponse oscillations (left axis) obtained at $V_g = 0.3$ V and under 360 GHz excitation from a Backward Wave Oscillator (BWO). A clear shift of around $\pi/2$ is observed that relates the response to the oscillation of the plasma waves in the channel. This gives strong evidence in favor of the detection mechanism proposed in Ref. [18].

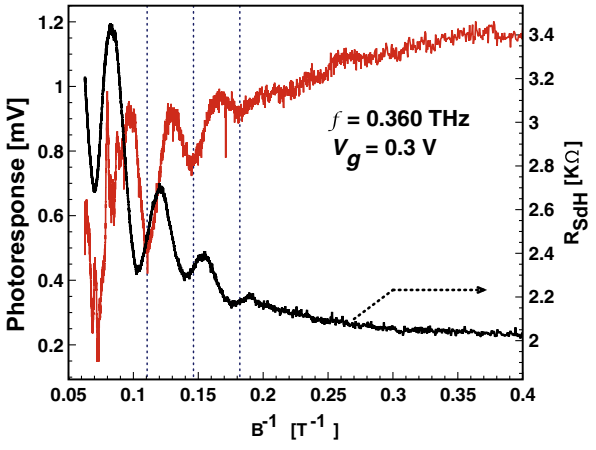

Fig. 4. Shubnikov-de-Haas oscillations (right axis) and photoresponse oscillations (left axis) as a function of magnetic field. The device was excited at low temperature (4 K) by BWO at 360 GHz and for a fixed gate bias ($V_g = 0.3$ V).

4. Terahertz imaging

The observed non-resonant response shows a relatively high signal to noise ratio (Fig. 3) and a low noise equivalent power (~1 $pW/Hz^{1/2}$), which allows the use of this device as a sensor for applications like terahertz imaging. Fig. 5 describes schematically the terahertz imaging system used. An electronic source based on frequency multipliers diode was used as a source of terahertz radiation at $f = 0.292$ THz. The radiation is collimated and focused by off-axis parabolic mirrors. Visible red LED in combination with an indium tin oxide (ITO) mirror[3] is used for the alignment of the Terahertz beam. The incident THz light is mechanically chopped at 333 Hz, and the photo-induced drain-to-source voltage ΔU is measured using a lock-in technique. All measurements were done at room temperature and under atmospheric pressure. Computer for image capture controls both the XY stage of the sample and the lock-in amplifier. More information about the terahertz imaging system setup can be found in [9].

The gate bias (V_g) was fixed at a value close to the threshold voltage to obtain optimum signal for imaging and high values of the signal to noise ratio. Fig. 6 shows both visible (up) and terahertz image (down) of a plastic box with a hidden mirror. The resolution of the image is 125 × 333 pixels and was obtained using the Si/SiGe MODFET with $L_g = 250$ nm as the terahertz sensor. The shapes of the mirror and box are easily identified in the image. The inner part shows less absorption because the material is semi-transparent to terahertz radiation. Figs. 7 and 8 show respectively the terahertz images of a VISA card with a resolution of 153 × 333 pixels obtained using the same transistor and a cigarette box with a resolution of 133 × 333 pixels obtained using the Si/SiGe MODFET with $L_g = 50$ nm. In the case of the cigarette box, most of the terahertz radiation is absorbed by the inner cover of the package made of aluminum. However, we can clearly distinguish three cigarettes present inside the box. For the VISA card image, the plastic part shows higher intensity of the signal and the chip (covered by the copper contacts) as well as the numbers and the dove hologram (lower-left part) absorbed most of the light. In this image, the rear part of the card (signature panel) is also visible. Those images demonstrate the capability of Si/SiGe MOSFETs to build compact terahertz imaging systems and their potential role in other terahertz applications. Those systems are inexpensive, compact, operate at room temperature and can be monolithically integrated along with Si-circuitry.

5. Resonant detection

Fig. 9a shows the photoresponse signal as a function of gate bias for a device with a gate length of 250 nm under BWO excitation at two frequencies 323 and 360 GHz. The measurements were performed at 4 K where high mobility and a high quality factor of the plasma oscillation are obtained. A clear shift of the peak response to higher gate voltages with excitation frequency was ob-

[3] Transparent for the red LED radiation and highly reflective for the Terahertz beam

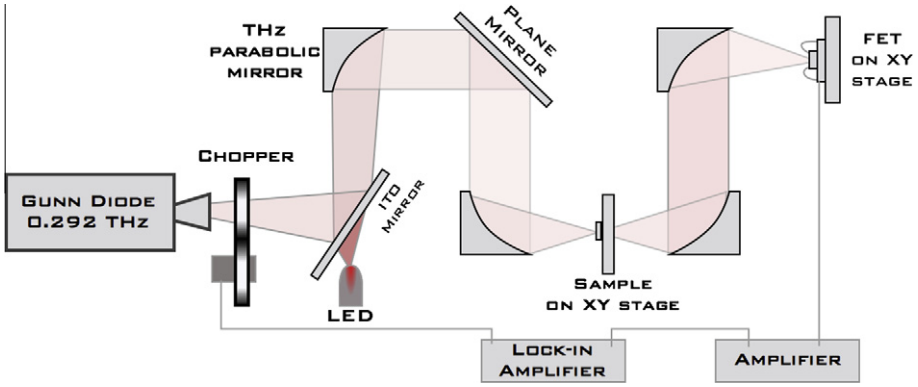

Fig. 5. Schematic description of the experimental setup of the imaging system.

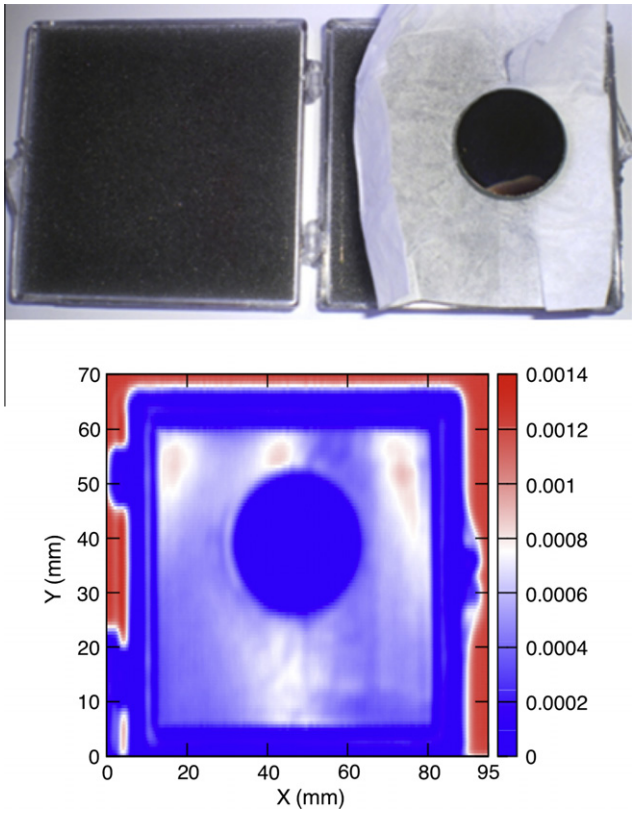

Fig. 6. Visible (up) and terahertz image (down) of a plastic box with a hidden mirror inside obtained using Si/SiGe MODFET with L_g = 250 nm.

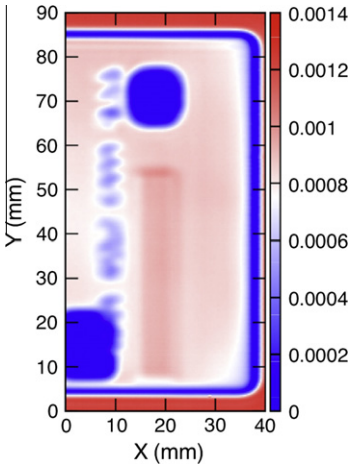

Fig. 7. Terahertz image of a VISA card obtained using Si/SiGe MODFET with L_g = 250 nm.

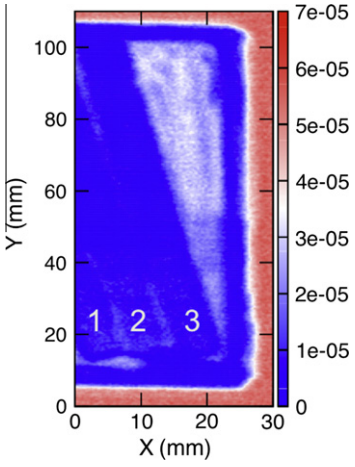

Fig. 8. Terahertz image of a cigarette box where tree cigarettes are present in the box obtained using Si/SiGe MODFET with L_g = 50 nm.

served. The square and diamond symbols in Fig. 9b mark the maximum of signals at 323 and 360 GHz, respectively, that have been obtained experimentally. According to the Dyakonov–Shur theory [19], the resonance frequency can be tuned by the gate bias and is given by:

$$F_0 = \frac{1}{4L_g}\sqrt{\frac{eU_0}{m^*}} \tag{5}$$

where $U_0 = U_g - U_{th}$, U_g is the gate-to-channel voltage, and U_{th} is the threshold voltage at which the channel is completely depleted, L_g is the gate length, and m^* is the effective mass of electrons. Note that Eq. (5) is valid under the gradual channel approximation. The resonant frequency as a function of the voltage swing is plotted for L_g = 230 nm (Fig. 9b) for which a better fit is obtained. The displacement toward higher gate voltages is in good agreement within the Dyakonov–Shur theoretical prediction.

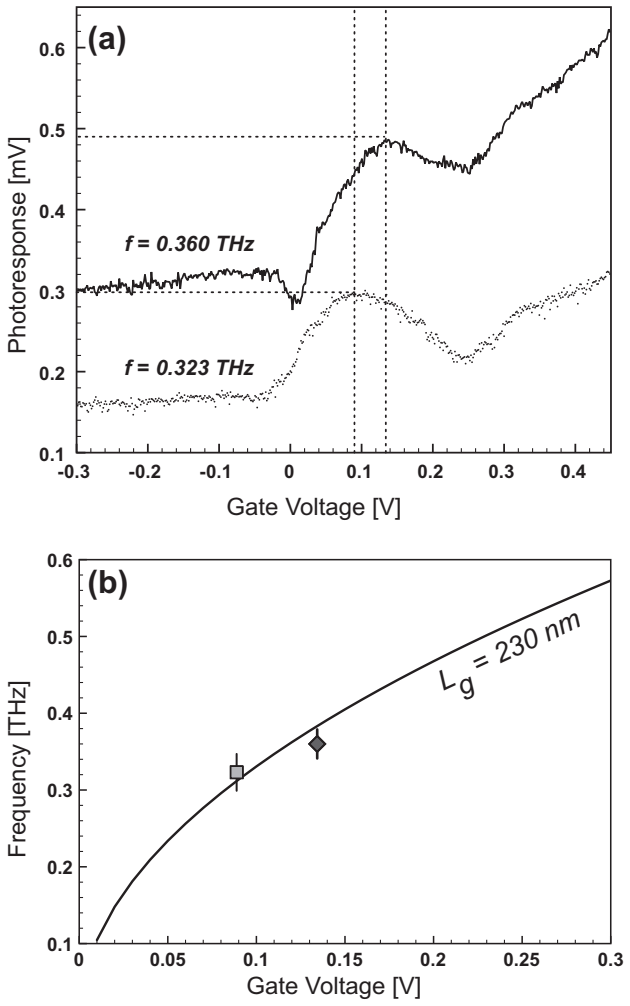

Fig. 9. (a) Photoresponse vs gate bias at two frequencies of the incoming radiation (323 and 360 GHz). (b) Resonance frequency vs swing voltage for L_g = 230 nm gate lengths.

6. Conclusion

We reported on resonant and non-resonant detection of terahertz radiation using strained-silicon modulation doped field effect transistors of two different gate lengths. The terahertz response was related to the oscillations of the plasma waves in the channel. Additionally, we have demonstrated the capabilities of these devices in terahertz imaging, this opens the way to design and use Si/SiGe devices in different applications in terahertz technology.

Acknowledgments

Devices were kindly supplied by Dr. T. Hackbarth. Authors from Salamanca University acknowledge the financial support from the Ministry of Science and Innovation (MICINN) through the projects PPT-120000-2009-4, PCT-420000-2010-008 and TEC2008-02281 and Junta de Castilla y León (Grants Numbers SA061A09 and SA049A10). Y.M.M. thanks Prof. T. Otsuji from Tohoku University in Japan for the help in experiments and fruitful discussions. Authors from Montpellier University acknowledge the support from ANR project "WITH", CNRS, and GDR-I project "Semiconductor sources and detectors of THz frequencies" in the framework of the "GIS Teralab". Thanks to Region of Languedoc-Roussillon through the "Terahertz Platform" project.

References

[1] Tonouchi M. Cutting-edge terahertz technology. Nat Photon 2007;1:97–105. http://dx.doi.org/10.1038/nphoton.2007.3.
[2] Siegel P. Terahertz technology. IEEE Trans Microwave Theory Tech 2002;50(3):910–28.
[3] Dyakonov M, Shur M. Detection mixing and frequency multiplication of terahertz radiation by two-dimensional electronic fluid, electron devices. IEEE Trans Electron Dev 1996;43(3):380–7. http://dx.doi.org/10.1109/16.485650.
[4] Knap W, Deng Y, Rumyantsev S, Lü J-Q, Shur MS, Saylor CA, et al. Resonant detection of subterahertz radiation by plasma waves in a submicron field-effect transistor. Appl Phys Lett 2002;80(18):3433–5. http://dx.doi.org/10.1063/1.1473685.
[5] Knap W, Kachorovskii V, Deng Y, Rumyantsev S, Lü J-Q, Gaska R, et al. Nonresonant detection of terahertz radiation in field effect transistors. J Appl Phys 2002;91(11):9346–53. http://dx.doi.org/10.1063/1.1468257.
[6] Knap W, Teppe F, Meziani Y, Dyakonova N, Lusakowski J, Boeuf F, et al. Plasma wave detection of sub-terahertz and terahertz radiation by silicon field-effect transistors. Appl Phys Lett 2004;85(4):675–7. http://dx.doi.org/10.1063/1.1775034.
[7] Meziani YM, Lusakowski J, Dyakonova N, Knap W, Seliuta D, Sirmulis E, et al. Non resonant response to terahertz radiation by submicron CMOS transistors. IEICE Trans Electron 2006;E89-C:993–8.
[8] Tauk R, Teppe F, Boubanga S, Coquillat D, Knap W, Meziani YM, et al. Plasma wave detection of terahertz radiation by silicon field effects transistors: responsivity and noise equivalent power. Appl Phys Lett 2006;89(25):253511. http://dx.doi.org/10.1063/1.2410215.
[9] Schuster F, Coquillat D, Videlier H, Sakowicz M, Teppe F, Dussopt L, et al. Broadband terahertz imaging with highly sensitive silicon CMOS detectors. Opt Express 2011;19(8):7827–32. http://dx.doi.org/10.1364/OE.19.007827, http://www.opticsexpress.org/abstract.cfm?URI=oe-19-8-7827.
[10] Ö jefors E, Lisauskas A, Glaab D, Roskos H, Pfeiffer U. Terahertz imaging detectors in CMOS technology. J Infrared Millimeter Terahertz Waves 2009;30:1269–80. http://dx.doi.org/10.1007/s10762-009-9569-4.
[11] Lisauskas A, Pfeiffer U, Ö jefors E, Bolvar PH, Glaab D, Roskos HG. Rational design of high responsivity detectors of terahertz radiation based on distributed self-mixing in silicon field-effect transistors. J Appl Phys 2009;105(11):114511. http://dx.doi.org/10.1063/1.3140611.
[12] Rumyantsev SL, Fobelets K, Veksler D, Hackbarth T, Shur MS. Strained-Si modulation doped field effect transistors as detectors of terahertz and sub-terahertz radiation. Semiconductor Science and Technology 2008;23(10):105001. http://stacks.iop.org/0268-1242/23/i=10/a=105001.
[13] Minamide H, Ikari T, Ito H. Frequency-agile terahertz-wave parametric oscillator in a ring-cavity configuration. Rev Sci Instrum 2009;80(12):123104. http://dx.doi.org/10.1063/1.3271039.
[14] Stillman WJ, Shur MS. Closing the gap: plasma wave electronic terahertz detectors. J Nanoelectron Optoelectron 2007;2(3):209–21.
[15] Veksler D, Teppe F, Dmitriev AP, Kachorovskii VY, Knap W, Shur MS. Detection of terahertz radiation in gated two-dimensional structures governed by dc current. Phys Rev B 2006;73:125328. http://dx.doi.org/10.1103/PhysRevB.73.125328.
[16] Meziani YM, Garcia E, Velazquez E, Diez E, Moutaouakil AE, Otsuji T, et al. Strained silicon modulation field-effect transistor as a new sensor of terahertz radiation. Semicond Sci Technol 2011;26(10):105006. http://stacks.iop.org/0268-1242/26/i=10/a=105006.
[17] Drexler C, Dyakonova N, Olbrich P, Karch J, Schafberger M, Karpierz K, et al. Helicity sensitive terahertz radiation detection by field effect transistors 2012;111:124504.
[18] Lifshits MB, Dyakonov MI. Photovoltaic effect in a gated two-dimensional electron gas in magnetic field. Phys Rev B 2009;80:121304. http://dx.doi.org/10.1103/PhysRevB.80.121304.
[19] Dyakonov M, Shur MS. Plasma wave electronics for terahertz applications. In: Miles R, Harrison P, Lippens D, editors. Terahertz sources and systems. Netherland: Kluer Academic Publishers; 2001. p. 187–207.